Modeling dipolar and quadrupolar defect structures generated by chiral islands in freely suspended liquid crystal films

N. M. Silvestre,[1,2,*] P. Patrício,[3,2] M. M. Telo da Gama,[1,2]
A. Pattanaporkratana,[4,5] C. S. Park,[4] J. E. Maclennan,[4] and N. A. Clark[4]
[1]*Departamento de Física da Faculdade de Ciências, Universidade de Lisboa, Avenida Professor Gama Pinto 2, P-1649-003 Lisboa Codex, Portugal*
[2]*Centro de Física Teórica e Computacional, Universidade de Lisboa, Avenida Professor Gama Pinto 2, P-1649-003 Lisboa Codex, Portugal*
[3]*Instituto Superior de Engenharia de Lisboa, Rua Conselheiro Emídio Navarro 1, P-1949-014 Lisboa, Portugal*
[4]*Department of Physics and Liquid Crystal Materials Research Center, University of Colorado, Boulder, Colorado, 80309 USA*
[5]*Physics Department, Kasetsart University, Bangkok 10900, Thailand*
(Received 29 April 2009; published 30 October 2009)

We report a detailed theoretical analysis of quadrupolar interactions observed between islands, which are disklike inclusions of extra layers, floating in thin, freely suspended smectic-*C* liquid crystal films. Strong tangential anchoring at the island boundaries results in a strength +1 chiral defect in each island and a companion −1 defect in the film—these forming a topological dipole. While islands of the same handedness form linear chains with the topological dipoles pointing in the same direction, as reported in the literature, islands with different handedness form compact quadrupolar structures with the associated dipoles pointing in opposite directions. The interaction between such heterochiral-island-defect pairs is complex, with the defects moving to minimize the director field distortion as the distance between the islands changes. The details of the interisland potential and the trajectories of the −1 defects depend strongly on the elastic anisotropy of the liquid crystal, which can be modified in the experiments by varying the material chirality of the liquid crystal. A Landau model that describes the energetics of freely mobile defects is solved numerically to find equilibrium configurations for a wide range of parameters.

DOI: 10.1103/PhysRevE.80.041708 PACS number(s): 61.30.Jf, 61.30.Dk

I. INTRODUCTION

The interactions between colloidal particles, fluid drops, and phase-separated domains in liquid crystals (LCs) are mediated by the distortion of the ordered fluid and depend on the LC elastic constants as well as on the anchoring conditions at the inclusion boundaries. The tendency of such inclusions to form aggregates depends intimately on the properties of the inclusions as well as those of the LC, providing exquisite control of the self-assembled colloidal structures. A key feature of these systems is the presence of topological defects, which are singularities of the LC director field, close to the boundaries of the inclusions. In the strong anchoring regime, the director field is distorted from its equilibrium uniform state near each inclusion and, in general, topological constraints lead to a distortion equivalent to that of a virtual +1 defect inside the inclusion. In order to match the uniform director field far away, one or more defects of opposite sign are nucleated in the liquid crystal matrix, outside the inclusion. The nature of these defects determines the symmetry of the director field around inclusions and their long-range interactions, for example, whether they are dipolar or quadrupolar. The short-range interactions are more difficult to predict as the defects may move when the inclusions approach each other, leading to complex two-body interactions.

When small spherical particles are suspended in three-dimensional (3D) nematics [1], several beautiful colloid-defect structures are observed [2,3], including the "satellite" (a single −1 defect next to an inclusion with radial anchoring) [4–6], "Saturn ring" (a defect line around an inclusion with radial anchoring) [7], and "boojum" (a pair of strength 1/2 defects at the poles of inclusions with tangential anchoring) configurations [8]. The director field around the inclusion-defect pair typically has dipolar or quadrupolar symmetry [9], leading to a variety of self-organized superstructures [10–12].

In two dimensions (2Ds), the first experimental observation of inclusions of nematic droplets in chiral smectic-*C* (Sm-*C*) films reported radial anchoring of the director at the droplet boundaries and single −1 defects nearby [13]. Later observations of nematic and isotropic inclusions in achiral Sm-*C* smectic films reported tangential anchoring [14–17], and either one pair of −1/2 defects or a single −1 defect at the inclusion boundaries. More recently, a temperature-dependent tangential to radial anchoring transition at inclusion boundaries in chiral smectics with small spontaneous polarization was observed [18–20], resulting in positional rearrangements of the defects along the inclusion boundaries.

In principle, 2D systems of inclusions are simpler to model numerically than 3D systems as the computations required to calculate inclusion interactions coupled to mobile defects are considerably less demanding. Accurate simulations of a variety of 2D systems have been reported over a wide range of physical parameters. Important analytical developments based on techniques such as series expansions [21], electromagnetic analogies [22], and complex analysis [23] have provided a wealth of detailed information that

*Electronic address: nunos@cii.fc.ul.pt

complements the numerical analysis and have been used to test the accuracy of the numerical results. The method of images was used recently in this context to calculate the long-range interactions between inclusions under a variety of conditions [24] and inclusion-defect pair configurations, at short and long range, have been calculated numerically with very high precision [25–27]. The models reveal that the short-range interactions between quadrupolar inclusions are complex, with the defects moving as the distance between the inclusions is changed. When the inclusions are close together, the defects are shared equally by the two inclusions at equilibrium [28], reminiscent of covalent atomic bonding where the electronic density peaks in the region between the atoms. (A similar "bonding" mechanism where a circular defect line is shared by two inclusions, creating some spectacular equilibrium configurations, was also predicted numerically and observed in 3D nematics [29,30].)

In this paper, we study the interactions between circular islands, which are disklike inclusions of extra layers, in freely suspended Sm-*C* films [31]. These films are structured in 2D fluid layers, with the liquid crystal molecules aligned along an average direction that is tilted from the layer normal. The projection of the molecular tilt on the plane of the layers defines a 2D vector, the so-called **c**-director. The aim of this work is to provide a quantitative description of recent observations of the interactions between topologically chiral islands in both chiral and achiral freely suspended Sm-*C* films, in which the existence of an important class of inclusion interactions not studied previously in either 2D or 3D, was revealed, namely interactions that depend on inclusion chirality [32]. The experiments showed that islands often form linear chains with the dipoles aligned along the chains, similar to earlier observations, but that heterochiral-island-defect pairs form a quadrupolar structure with the topological dipoles pointing in opposite directions. Indeed, both dipolar chains and quadrupolar assemblies may coexist on the same achiral Sm-*C* film, the local organization being determined by the topological chirality of the individual islands.

This paper is organized as follows. In Sec. II we briefly summarize the experimental results, highlighting those that will be compared with the numerical calculations. In Sec. III we present a Landau free-energy model that describes self-consistently the disposition of freely mobile defects in the film, and solve it numerically for a wide range of parameters in Sec. IV, where a detailed comparison with the observations is carried out. Finally, we discuss the results and summarize our conclusions in Sec. V.

II. EXPERIMENTAL RESULTS

Figure 1 illustrates characteristic equilibrium configurations of island-defect pairs (with $N \sim 20$ layers) interacting on a background film ($N=2$) of racemic MX8068 [33]. Strong orientational anchoring at the island boundaries induces a +1 defect inside each island and −1 defects in the background film, each island-defect pair forming a topological dipole [inset, Fig. 1(a)]. Such dipoles attract over long distances through an elastic dipole-dipole interaction and, when the islands are sufficiently close, reach an equilibrium

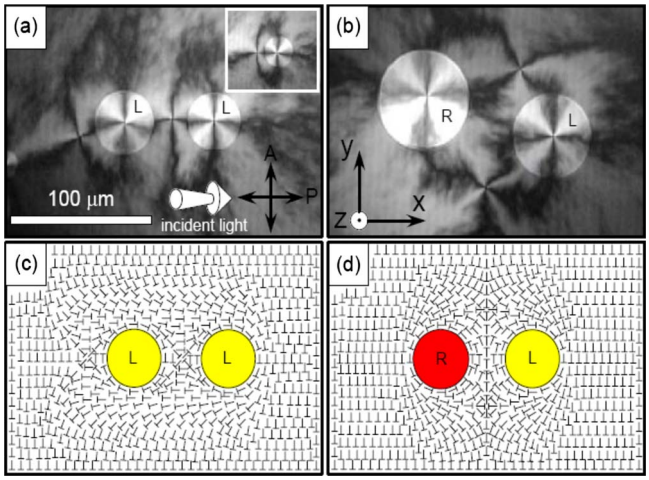

FIG. 1. (Color online) Chiral islands in a freely suspended smectic film of achiral liquid crystal. Depolarized reflected light microscope (DRLM) images of a smectic-*C* film of racemic MX8068 showing (a) two islands containing +1 defects with the same handedness and (b) two islands with +1 defects of opposite handedness. Each +1 defect is accompanied by a −1 defect in the film. The defects in (a) form a dipolar chain, while those in (b) form a topological quadrupole. The inset in (a) shows a single island with a +1 defect inside and a matching −1 defect in the background film, the pair forming a dipole. The laser illumination (shown by the arrow) is obliquely incident in the *x*-*z* plane, allowing us to differentiate between left- and right-handed islands by comparing the brightness of the brushes in their upper and lower halves. The equilibrium **c**-director field (⊢) is shown around two islands with (c) the same handedness and (d) opposite handedness, with the head of the ⊢ indicating the end of the molecule closer to the viewer.

separation where the elastic distortion is minimized. Two types of island-defect pairs are observed: either the pairs form linear chains with the dipoles pointing in the same direction along the chain, as in Fig. 1(a), or the dipoles point in opposite directions and the island-defect pairs form a quadrupolar structure, with the −1 defects placed symmetrically above and below the line joining the islands, as in Fig. 1(b). A sketch of the equilibrium **c**-director field when two islands with the same handedness are close to each other is shown in Fig. 1(c), while when the islands are heterochiral, the quadrupolar structure shown in Fig. 1(d) is favorable [32].

The equilibrium center-to-center separation D of islands of radius R in dipolar chains was found experimentally to be close to $2\sqrt{2}R$, the value predicted theoretically and confirmed in simulations using a free energy with a single elastic constant [22,26]. Islands in the quadrupolar structure also exhibit a well-defined equilibrium separation. When the island separation is altered using optical tweezers [34], the vertical separation S of the −1 defects also changes. At sufficiently large island separation, the quadrupolar symmetry is broken and the structure evolves into two separate dipoles [32].

The interaction between islands on an $N=2$ achiral Sm-*C* film was found to be weak, with large orientational fluctuations of the **c**-director leading to large fluctuations in the position of the −1 defect. In chiral MX8068 Sm-C^* films, in contrast, director fluctuations are smaller and the interaction

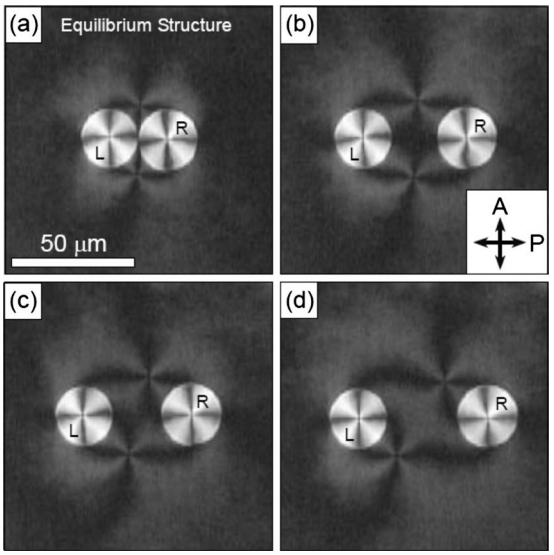

FIG. 2. Textures of heterochiral islands interacting on a film of 25% chirally doped MX8068. (a) The quadrupolar structure is in equilibrium when the islands almost touch. (b) The equilibrium separation between −1 defects increases as the islands are separated using optical tweezers. (c) When the separation is sufficiently large, the quadrupolar symmetry is broken. (d) When the islands are forced even further apart, the quadrupole evolves into two separate dipoles.

between islands is large enough to be measured using optical tweezers. On such chiral films, all of the islands are topologically homochiral and they form only dipolar chains. We propose that the reason for this bias is that the spontaneous polarization of the chiral Sm C^* phase prefers to point toward the liquid-crystal–air interface at the edges of the islands, inducing only left-handed +1 defects. In chiral films polarization is accompanied by a preferred sign of local band of the c-director [35,36]. If the boundary condition on c is tangential to the island surface then this preferred bend will be favored, selecting one handedness of the c-director field in and around the island and one direction of polarization normal to the island surface. In films of racemic MX8068 doped with a small amount of chiral material, left-handed defects predominate but some right-handed ones are also observed. At 25% chiral fraction, for example, about 1% of the observed defects are right handed. At this chiral fraction, the quadrupolar structure is found to be in equilibrium when the islands nearly touch [see Fig. 2(a)].

Optical tweezers may be used to displace the islands from their equilibrium separations. As illustrated in Figs. 2(b)–2(d), the equilibrium positions of the −1 defects change simultaneously as the islands are separated. In Fig. 3 we show the experimentally measured vertical separation S of the −1 defects as a function of the island center-to-center separation D for racemic and 25% chiral fraction films, plotted together with theoretical results to be described in the next section.

III. ELASTIC FREE ENERGY OF SMECTIC-C LAYERS

The molecular orientation in smectic-C free standing films may be described by the **c**-director, a two-dimensional

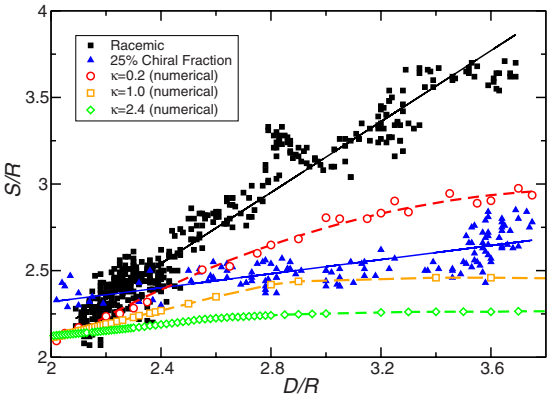

FIG. 3. (Color online) Equilibrium vertical separation S of the −1 defects as a function of the island center-to-center separation D in the quadrupolar configuration regime, for racemic and 25% chirally doped films of MX8068, compared with the results of numerical calculations for systems with elastic anisotropies $\kappa=0.2$, 1.0, and 2.4. The straight lines are linear fits of the experimental data. The dashed lines are fits to the numerical data shown here to guide the eye. The value of $\kappa=2.4$ was chosen to reproduce the slope of the linear fit for the chiral mixture. Experimental textures [32,40] indicate that the chiral mixture should correspond to $\kappa \approx 1.0$. Note, however, that the theoretical results for this κ underestimate the value of S/R at contact ($D/R=2$). Fluctuations are expected to increase the average defect separation, S, and account, at least in part, for this discrepancy. The average slope of the experimental data for the racemate is high, indicating very small values of κ, a limit which is numerically inaccessible in our simulations.

unit vector field $\mathbf{c}=(\cos\theta,\sin\theta)$ in the direction of the in-plane projection of the average molecular tilt. The total elastic free energy $\mathcal{F}$ of a film of thickness ℓ may be written as the sum of two terms,

$$\mathcal{F}=\ell\int_{\Omega} f_{\mathbf{c}}\,dxdy+\ell\int_{\partial\Omega} f_w\,ds, \tag{1}$$

where Ω is the area of the liquid crystal film, and $\partial\Omega$ its boundary, including any inclusion boundaries that may be present. The second term accounts for anchoring at the boundaries and may be omitted in the strong anchoring regime. The first term describes the macroscopic free-energy cost of elastic distortions of the smectic-C-director field and is given by

$$f_{\mathbf{c}}=\frac{1}{2}(\mathcal{K}_s(\nabla\cdot\mathbf{c})^2+\mathcal{K}_b(\nabla\times\mathbf{c})^2), \tag{2}$$

where $\mathcal{K}_s$ and $\mathcal{K}_b$ are respectively the 2D splay and bend elastic constants.

This macroscopic elastic free energy neglects variations of the degree of liquid crystalline order and it is inadequate when disordering effects are important. This is the case when topological defects are present, as the order vanishes at the center of the defects. A better approach, which is also more tractable numerically, is to use a mesoscopic description that takes into account variations of the degree of order on the scale of the relevant correlation length. This is accomplished

by theories of the Landau class that consider the free energy as a functional of a generalized order parameter, a quantity with the symmetry of the distortion field (*XY* or 2D vector in this case) that is nonzero in the ordered phase and vanishes in the disordered phase. This order parameter varies throughout a nonuniform system and is capable of describing the inhomogeneities in orientation and degree of order that occur at topological defects. If we replace the two-dimensional director field $\mathbf{c}=(c_x,c_y)$ by the complex order parameter $\phi=\phi_x+i\phi_y=|\phi|(c_x+ic_y)$, we may write the bulk free energy (in reduced units [37]) as

$$\mathcal{F}=\int_\Omega f_\phi dxdy, \tag{3}$$

with energy density

$$f_\phi=|\phi|^2(|\phi|^2-1)+\xi^2[(\partial_x\phi_x+\partial_y\phi_y)^2+\kappa(\partial_x\phi_y-\partial_y\phi_x)^2], \tag{4}$$

where ξ is the correlation length [37] (the characteristic size of the inhomogeneities), and $\kappa=\mathcal{K}_b/\mathcal{K}_s$ the ratio of the elastic constants. This free energy includes all scalar invariants of both the order parameter (up to fourth order in $|\phi|$) and its derivatives. The negative sign of the quadratic term in ϕ indicates that the stable, uniform phase is ordered and in the absence of constraints the free energy is minimized by a uniform field of magnitude $|\phi|=1/\sqrt{2}$. When the direction of ϕ varies in space, its magnitude may also change in order to minimize the total free energy. At the defects, the order parameter ϕ varies rapidly, its magnitude vanishing within a distance of the order of the temperature-dependent correlation length ξ.

In chiral films, the director field is additionally coupled to the free energy associated with the local space charge $-\nabla\cdot\mathbf{P}$, where $\mathbf{P}$ is the spontaneous polarization, and is affected by screening from impurity ions dissolved in the film. We assume here that the effect of material chirality of the LC may be described by increasing the effective bend elastic constant, $\mathcal{K}_b$, or, equivalently, by increasing the ratio of the elastic constants, κ [35,38].

IV. SIMULATION RESULTS

In this section we present detailed numerical results describing the interaction between homochiral and heterochiral islands for a range of parameters. In particular, we calculate the separation of the two −1 defects associated with a pair of heterochiral islands as a function of the island separation and compare this with the experimental results to obtain an estimate of the effective elastic anisotropy of the experimental systems.

We start by considering two islands with strong (fixed) tangential anchoring conditions, and the same handedness. For simplicity, we have taken $|\phi|=1/\sqrt{2}$, the bulk equilibrium value of the order parameter for uniform alignment, at the island boundaries. At the borders of the domain, representing large distances, we have forced the director to be uniformly aligned along the *y* direction. The correlation length that sets the scale for the size of the defects was taken

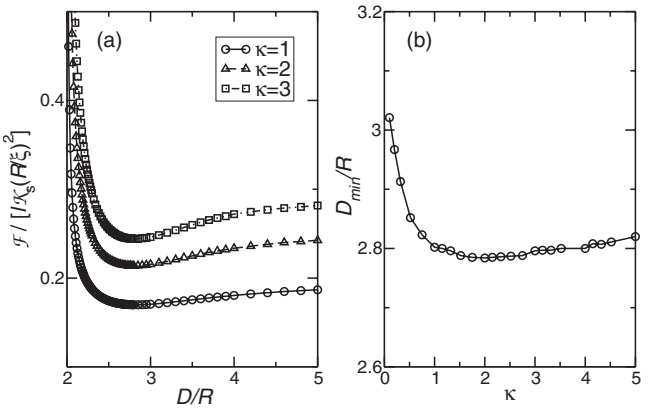

FIG. 4. (a) Total free energy as a function of homochiral island separation *D*, for different κ. When $\kappa=\mathcal{K}_b/\mathcal{K}_s=1$, the free energy exhibits a minimum at a separation $D_{\min}=2\sqrt{2}R$. (b) Equilibrium separation $D_{\min}$ as a function of the elastic anisotropy κ of the system.

to be $\xi=0.1R$, a tenth the radius of the circular islands, *R*, which were assumed to be monodisperse. This is admittedly an overestimate of the actual defect size but the major difficulty in the numerical analysis stems from the disparity in the length scales *R* and ξ, and this choice is a compromise that speeds up the calculations and allows a systematic investigation of a wide range of systems. We have carried out calculations for a smaller value of $\xi=0.01$, showing that the computed island/defect textures depend overwhelmingly on the ratio κ, with little dependence on the core size. As in previous work [26], we have used finite elements with adaptive meshing to minimize the free energy. A first triangulation respecting the predefined boundaries is constructed. The order parameter ϕ is specified at the vertices of the mesh and linearly interpolated within each triangle. The free energy is then minimized using standard methods, the Hessian of the solution at each iteration being used to generate a new mesh. If the solution presents stronger spatial variations (usually near the defects), a mesh refinement is required. On the contrary, if the solution is almost constant over a large region (far from the islands, for example), a coarsening of the mesh is possible. In typical calculations, convergence is obtained after only two mesh adaptations, corresponding to final meshes with 6×10^3 points, spanning a region of $15R\times15R$, and minimal mesh sizes of $10^{-4}R$ close to the defects. The free energy is obtained with a relative accuracy of 10^{-4}.

We have calculated the free energy of a pair of homochiral islands forming a chain with their satellite −1 defects as a function of the island center-to-center separation *D*. In order to investigate the effects of the elastic anisotropy, κ was varied over a wide range. We see from Fig. 4(a) that the interaction between two islands is attractive at long distances, exhibits a well-defined minimum, and is repulsive at small distances. For $\kappa=1$, the equilibrium separation $D_{\min}=2.80R$ is slightly different from that obtained in our previous work, $D_{\min}=2.82R$, based on Frank elastic free energy (1) with no order-parameter variation and pinned defects [26]. This difference is a consequence of the larger value used for ξ here. Nevertheless, in order to carry out extensive calculations and explore a reasonable range of parameters,

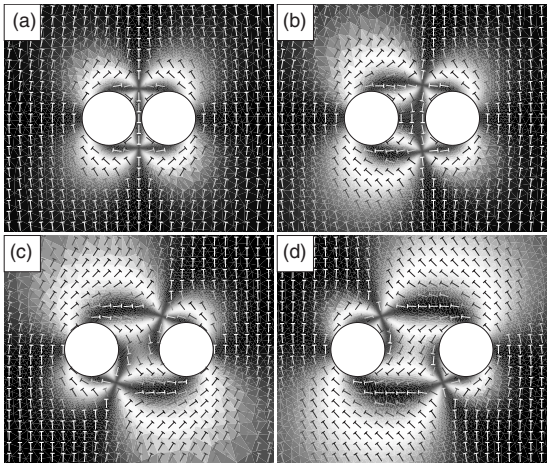

FIG. 5. Equilibrium director configurations for different heterochiral-island separations with $\kappa=1$. (a) $D=2.2R$: the defects are equally shared by the islands, in a symmetric, quadrupolar configuration. (b) $D=3.0R$: the symmetry is broken; here the defects are found in a metastable configuration where they are both closer to one island. (c) $D=3.5R$: each defect follows a different island. (d) $D=4.0R$: even at this separation, the positions of the defects are still strongly influenced by the presence of the other island-defect pair, with configurations typical of isolated dipoles occurring at larger separations.

we decided to keep $\xi=0.1R$, as the discrepancy in theoretical equilibrium distances obtained is small compared with the uncertainty in the experimental data. The equilibrium separation $D_{\min}$ as a function of κ is plotted in Fig. 4(b), showing the separation increasing sharply as the bend elasticity is reduced below $(\kappa \to 0)$ but approximately constant for $\kappa \gtrsim 1$.

We next considered two islands with opposite handedness, with the defects located between them as observed in the experiments and shown in Fig. 2. In this case, the defects strongly influence the interaction between the islands, and they move considerably as the distance between the islands changes. As a result, the number of mesh adaptations had to be increased to three or four in order to obtain reasonably accurate results (indicated by the smoothness of the free-energy plots, for example). Figures 5 and 6 illustrate model director configurations for different island separations D for systems characterized by two different elastic anisotropies, $\kappa=1$ and $\kappa=0.2$. When the islands are very close together, the defects are located symmetrically in a quadrupolar structure, being shared equally by the two islands [Figs. 5(a), 6(a), and 6(b)]. Above a certain island separation, this symmetry is broken and each defect becomes associated primarily with just one of the islands. We also sometimes observe configurations in which both defects are closer to the same island [see Fig. 5(b)], although these are metastable. The defects influence each other over large distances [Figs. 5(c), 5(d), 6(c), and 6(d)], their relative positions with respect to their parent islands being very different from an isolated island-defect configuration. When the elastic anisotropy of the liquid crystal is large, the defect brushes become sharper [39], as shown in Fig. 6 for the case $\mathcal{K}_s=5\mathcal{K}_b$ $(\kappa=0.2)$. The interaction between the islands is, however, qualitatively similar to the isotropic elasticity case.

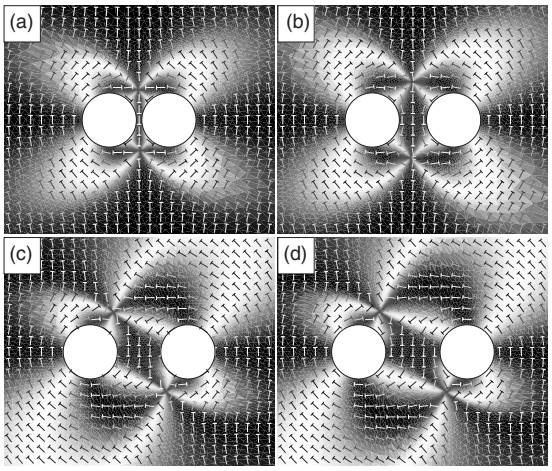

FIG. 6. Equilibrium director configurations for different heterochiral-island separations with $\kappa=0.2$. The order parameter around the -1 defects has no longer a circular symmetry as in Fig. 5. This is reflected in the narrowness of the white brushes that come out of the -1 defects. (a) $D=2.2R$. (b) $D=3.0R$. (c) $D=3.5R$. (d) $D=4.0R$.

The effect of elastic anisotropy on the interaction between two
heterochiral islands was investigated by calculating the free energy as a function of the center-to-center island separation, D, for different values of κ. The results are plotted in Fig. 7(a). For small κ, the potential is similar to that observed with homochiral islands [Fig. 4(a)] but the equilibrium separation is smaller and decreases monotonically with κ, as shown in Fig. 7(b). The islands are much closer together than in the homochiral case and when κ is large, the islands almost touch each other, as observed in the experiments [32].

We next studied the geometric evolution of heterochiral-island-defect pairs as the island separation was varied. In particular, we tracked the vertical separation of the -1 defects as a function of the distance between islands in order to compare it with the experimental results and to estimate the effective elastic anisotropy of the experimental systems.

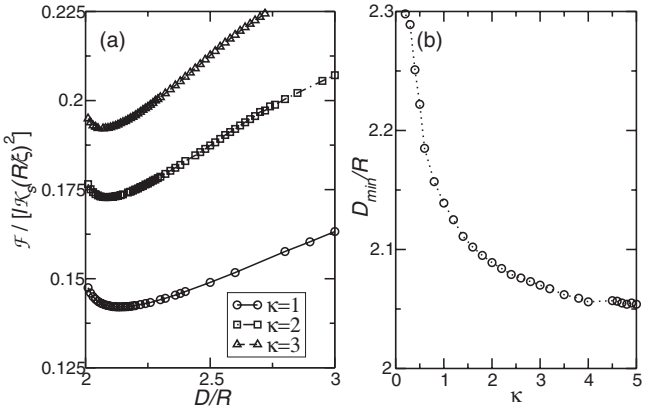

FIG. 7. (a) Total free energy as a function of heterochiral-island separation D, for $\kappa=\mathcal{K}_b/\mathcal{K}_s=1$, 2, and 3. All systems have a well-defined equilibrium separation $D_{\min}$ that is smaller than in the homochiral case and decreases monotonically with increasing κ (b).

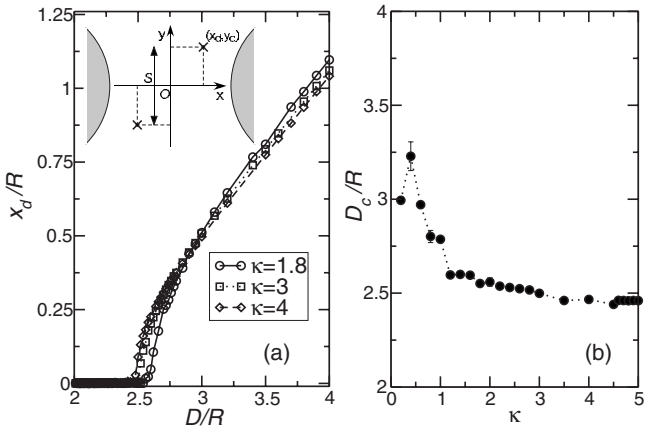

FIG. 8. (a) Computed horizontal position of the right defect x_d as a function of island separation D, for $\kappa=1.8$, 3.0, and 4.0. The reference system has its origin at the midpoint between the islands. (b) The quadrupolar symmetry of the island-defect pair is generally broken at a critical island separation D_c, shown here as a function of κ. The noisiness of the data when $\kappa<1$ reflects the numerical difficulties encountered in modeling this regime.

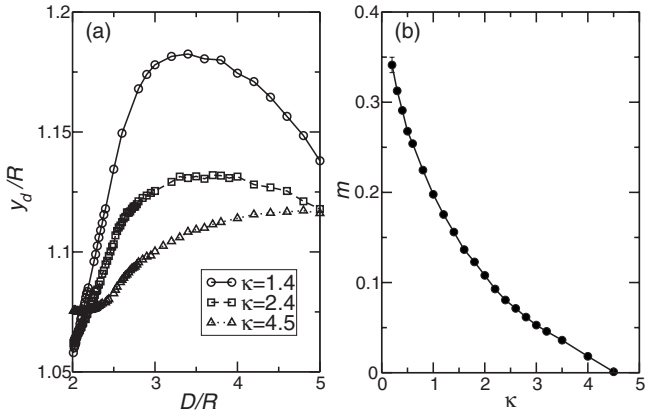

FIG. 9. (a) Computed vertical displacement y_d of the upper −1 defect as a function of island separation D, for $\kappa=1.4$, 2.4, and 4.5 [y_d is half the vertical defect separation S plotted in Fig. 3.] For small D (close to equilibrium), the displacement of the defect increases linearly with a well-defined slope m, shown in (b) as a function of the elastic anisotropy κ.

Determining the trajectories of the −1 defects as a function of island separation is computationally very demanding, as an accurate determination of the position of the defects requires a large number of mesh adaptations, and is particularly difficult at the quadrupolar symmetry-breaking transition, an effect we now describe. At small separations, the islands share the defects in a symmetric, quadrupolar configuration. In this regime, the defects are along the vertical bisector of the islands, so their horizontal coordinate $x_d=0$ [see Fig. 8(a)] but at a critical island separation, D_c, the quadrupolar symmetry is broken and x_d becomes nonzero. One of the defects moves to the right, acquiring a positive x_d offset, while the other moves symmetrically to the left and has negative x_d. This behavior is qualitatively the same for all values of the elastic anisotropy κ that were investigated, but the island separation at which the transition occurs depends on κ. Figure 8(b) shows the critical island separation D_c as a function of κ. The trend observed in D_c confirms that the quadrupolar symmetry is broken in a continuous transition, or bifurcation, that occurs at a precise value of the island separation.

Similarly, the vertical displacement of the defects y_d was determined as a function of D, with results shown in Fig. 9(a) for several values of κ. For moderately anisotropic systems ($\kappa=1.4$ and 2.4), the vertical displacement of the defects first increases, approximately linearly, as the island separation increases. When x_d bifurcates at $D_c\approx 2.5R$, however, the behavior of y_d changes, increasing to a maximum and then decreasing slowly, until it reaches the isolated island-defect value, $y_d=0$, at large separation. These results illustrate how strongly the island-defect pairs interact even at quite large distances: for $D\sim 5R$, the vertical displacement of the defects is still very large, $y_d\sim R$. The initial slope of the y_d vs. D curve, which is a measure of the susceptibility of y_d to fluctuations in the island separation, is plotted in Fig. 9(b) as a function of κ. For values smaller than $\kappa=0.2$, the numerical results become unreliable: although the energy can still be obtained accurately in this regime, the equilibrium defect positions are sensitive to numerical noise and cannot be uniquely defined. As the islands separate, the position of the defects may vary substantially, and due to the high degree of accuracy required for small κ, our method is not able to resolve them.

The numerical vertical separation of the defects, $S=2y_d$, were compared with the experimental results in Fig. 3. The value of $\kappa=2.4$ was chosen to reproduce the slope of the linear fit for the chiral mixture. Experimental textures [32,40] indicate that the 25% chiral mixture should correspond to $\kappa\approx 1.0$. Note, however, that the theoretical results for this κ underestimate the value of S/R at contact ($D/R=2$). Keeping the same κ, we decreased the correlation length ξ by a factor of ten. However, we still obtained a smaller value of S/R at contact. Fluctuations are expected to increase the average defect separation, S, and account, at least in part, for this discrepancy [24]. The average slope of the experimental data for the racemate is high, indicating very small values of κ, a limit that is numerically inaccessible in our simulations.

In principle, the susceptibility of the vertical displacement of the −1 defects to perturbations of the islands from their equilibrium separation plotted in Fig. 9(a) should allow an estimate of κ in the experiments. The calculations suggest a strong variation of this susceptibility as the elastic anisotropy κ changes, as shown in Fig. 9(b), but we have thus far been unable to reconcile the predicted behavior quantitatively with the experimental data.

V. CONCLUSION

We have described numerical simulations of the spontaneous quadrupolar symmetry breaking of the director field around heterochiral-island-defect pairs in Sm-*C* liquid crystal films. In these films, the **c**-director is tangentially anchored at the island boundaries, inducing a +1 defect inside each island and a −1 defect outside in the background film,

the island-defect pair forming a dipole. Such dipoles attract each other over long distances through an elastic dipole-dipole interaction and, when the islands are sufficiently close, reach an equilibrium separation where the overall elastic distortion is minimized.

Two types of island-defect pairs observed in the experiments were considered in the theoretical analysis. Either the islands have the same handedness, in which case they form linear chains with the dipoles pointing in the same direction along the chain, or the islands have different handedness and the dipoles point in opposite directions. In the latter case, at short distances, the island-defect pairs form a quadrupolar structure, with the -1 defects placed symmetrically above and below the line joining the islands.

The simulations show that interactions between two heterochiral islands occur over a much longer range than homochiral island-defect pairs. Even when the islands are separated by up to five times their radius, the interaction between heterochiral-island-defect pairs is still quite different from the long-range dipole-dipole interaction expected in the linear asymptotic regime, and an island-defect configuration significantly different from that expected for isolated dipolar pairs.

We have observed, both experimentally and numerically, a transition where the quadrupolar symmetry of the heterochiral-island system is broken. This occurs at a well-defined critical island separation that depends on the effective elastic anisotropy of the liquid crystal and the simulations suggest that the quadrupolar symmetry is broken continuously. For each system, characterized by an elastic anisotropy κ, a well-defined critical island separation was found where the defects are displaced symmetrically from the vertical midplane bisecting the islands. The island separation at which this transition occurs decreases smoothly as κ increases (at least for $\kappa \gtrsim 0.5$), giving further support to the existence of a bifurcation that delimits the quadrupolar configuration regime. The numerical calculations of the defect positions are computationally demanding, leading to somewhat noisy results for systems with small $\kappa < 1$. Furthermore, at the transition large thermal fluctuations of the director field are expected and were observed experimentally in racemic systems. Including their effects in the model will affect the location (and maybe even the nature) of the bifurcation predicted by our mean-field analysis.

At small island separations, the computed vertical displacement of the defects was found to increase linearly, in general agreement with experiment. The scatter in the experimental data strongly suggests that thermal fluctuations in the position of the defects are important even in the quadrupolar configuration regime and that these fluctuations should be taken into account in a full description of the symmetry-breaking transition. The simulations suggest that the initial slope of the S vs. D curve may be used to estimate the effective elastic anisotropy $\kappa = \mathcal{K}_b / \mathcal{K}_s$ of experimental systems. We have found, however, that a good fit to the slope underestimates the defect separation at contact. It is likely that thermal fluctuations, which increase the average separation between defects, are responsible for this discrepancy. Furthermore, the polydispersity of the islands may also affect the simulation results reported here. Heterochiral islands of different sizes do not exhibit perfect quadrupolar symmetry and this may result in a different behavior of the experimental defect separation. Islands with different sizes and the effect of thermal fluctuations will be investigated in future work.

ACKNOWLEDGMENTS

Financial support from the Foundation of the University of Lisbon and the Portuguese Foundation for Science and Technology FCT under Contracts No. POCI/FIS/58140/2004 and No. POCTI/ISFL/2/618 is gratefully acknowledged. N.M.S. acknowledges the support of FCT through Grant No. SFRH/BPD/40327/2007. The Colorado group was supported by NASA Grant No. NAG-NNC04GA50G and by NSF MRSEC Grant No. DMR 0213918.

[1] H. Stark, Phys. Rep. **351**, 387 (2001).
[2] P. Poulin, H. Stark, T. C. Lubensky, and D. A. Weitz, Science **275**, 1770 (1997).
[3] I. Muševič, M. Škarabot, U. Tkalec, M. Ravnik, and S. Žumer, Science **313**, 954 (2006).
[4] R. W. Ruhwandl and E. M. Terentjev, Phys. Rev. E **56**, 5561 (1997).
[5] T. C. Lubensky, D. Pettey, N. Currier, and H. Stark, Phys. Rev. E **57**, 610 (1998).
[6] H. Stark, Eur. Phys. J. B **10**, 311 (1999).
[7] Y. Gu and N. L. Abbott, Phys. Rev. Lett. **85**, 4719 (2000).
[8] P. Poulin and D. A. Weitz, Phys. Rev. E **57**, 626 (1998).
[9] B. I. Lev, S. B. Chernyshuk, P. M. Tomchuk, and H. Yokoyama, Phys. Rev. E **65**, 021709 (2002).
[10] J.-C. Loudet, P. Barois, and P. Poulin, Nature (London) **407**, 611 (2000).
[11] V. G. Nazarenko, A. B. Nych, and B. I. Lev, Phys. Rev. Lett. **87**, 075504 (2001).
[12] S. P. Meeker, W. C. K. Poon, J. Crain, and E. M. Terentjev, Phys. Rev. E **61**, R6083 (2000).
[13] P. Cluzeau, P. Poulin, G. Joly, and H. T. Nguyen, Phys. Rev. E **63**, 031702 (2001).
[14] P. Cluzeau, G. Joly, H. T. Nguyen, and V. K. Dolganov, Pis'ma Zh. Eksp. Teor. Fiz. **76**, 411 (2002) [JETP Lett. **76**, 3512002 (2002)].
[15] C. Völtz and R. Stannarius, Phys. Rev. E **70**, 061702 (2004).
[16] P. Cluzeau, F. Bougrioua, G. Joly, L. Lejcek, and H. T. Nguyen, Czech. J. Phys. **55**, 719 (2005).
[17] P. V. Dolganov and V. K. Dolganov, Phys. Rev. E **73**, 041706 (2006).
[18] P. V. Dolganov, H. T. Nguyen, G. Joly, V. K. Dolganov, and P. Cluzeau, Europhys. Lett. **76**, 250 (2006); P. V. Dolganov, H. T. Nguyen, E. I. Kats, V. K. Dolganov, and P. Cluzeau, Phys. Rev. E **75**, 031706 (2007).

[19] C. Bohley and R. Stannarius, Eur. Phys. J. E **23**, 25 (2007).
[20] J. Fukuda, Eur. Phys. J. E **24**, 91 (2007).
[21] S. V. Burylov and Y. L. Raikher, Phys. Rev. E **50**, 358 (1994).
[22] D. Pettey, T. C. Lubensky, and D. R. Link, Liq. Cryst. **5**, 579 (1998).
[23] C. Bohley and R. Stannarius, Eur. Phys. J. E **20**, 299 (2006).
[24] K. S. Korolev and D. R. Nelson, Phys. Rev. E **77**, 051702 (2008).
[25] J. Fukuda and H. Yokoyama, Eur. Phys. J. E **4**, 389 (2001).
[26] P. Patrício, M. Tasinkevych, and M. M. Telo da Gama, Eur. Phys. J. E **7**, 117 (2002).
[27] R. Yamamoto, Y. Nakayama, and K. Kim, J. Phys.: Condens. Matter **16**, S1945 (2004).
[28] M. Tasinkevych, N. M. Silvestre, P. Patrício, and M. M. Telo da Gama, Eur. Phys. J. E **9**, 341 (2002).
[29] O. Guzmán, E. B. Kim, S. Grollau, N. L. Abbott, and J. J. de Pablo, Phys. Rev. Lett. **91**, 235507 (2003).
[30] M. Ravnik, M. Škarabot, S. Žumer, U. Tkalec, I. Poberaj, D. Babič, N. Osterman, and I. Muševič, Phys. Rev. Lett. **99**, 247801 (2007).
[31] See C. Bohley and R. Stannarius, Soft Matter **4**, 683 (2008) for a recent review about inclusions in Sm-*C* films.
[32] A. Pattanaporkratana, C. S. Park, J. E. Maclennan, N. A. Clark, W. Thurmes, N. M. Silvestre, P. Patrício, and M. M. Telo da Gama (to be published).
[33] MX8068 was provided by Displaytech, Inc. and has the phase sequence $X \overset{-22\ °C}{\leftrightarrow}$ Sm-C(Sm-C^*) $\overset{60.5\ °C}{\leftrightarrow}$ Sm-$A^* \overset{78\ °C}{\leftrightarrow} N^* \overset{80.5\ °C}{\leftrightarrow}$ I).
[34] A. Pattanaporkratana, C. S. Park, J. E. Maclennan, and N. A. Clark, Ferroelectrics **310**, 275 (2004); www.e-lc.org
[35] R. B. Meyer, L. Liébert, L. Strzelecki, and P. Keller, J. Phys (Paris), Lett. **36**, L69 (1975).
[36] S. A. Langer and J. P. Sethna, Phys. Rev. A **34**, 5035 (1986).
[37] N. M. Silvestre, P. Patrício, and M. M. Telo da Gama, Phys. Rev. E **74**, 021706 (2006).
[38] J.-B. Lee, R. A. Pelcovits, and R. B. Meyer, Phys. Rev. E **75**, 051701 (2007).
[39] D. R. Link, N. Chattham, J. E. Maclennan, and N. A. Clark, Phys. Rev. E **71**, 021704 (2005).
[40] A. Pattanaporkratana, Ph.D. thesis, University of Colorado, 2008.